Hindawi
Shock and Vibration
Volume 2020, Article ID 8861971, 10 pages
https://doi.org/10.1155/2020/8861971

Research Article

Relationship between Fractal Dimension of Fragmentation Degree and Energy Dissipation of Rock-Like Materials under Initial Stress

Ying Xu,[1,2] Jinjin Ge,[1] Hailong Li,[3] Rongzhou Yang,[1] Kun Wang,[1] and Shi Hu[1]

[1]*School of Civil Engineering and Architecture, Anhui University of Science and Technology, Huainan 232001, Anhui, China*
[2]*Key Lab. of Coal Deep-Well Structural Technique, Huaibei 235000, Anhui, China*
[3]*School of Petroleum Engineering, China University of Petroleum (East China), Qingdao 266580, Shandong, China*

Correspondence should be addressed to Jinjin Ge; 157534201@qq.com

Received 28 September 2020; Revised 9 November 2020; Accepted 12 November 2020; Published 29 November 2020

Academic Editor: Pengfei Wang

In order to obtain the relationship between fractal dimension and energy dissipation of rock-like materials under initial stress state, a variable cross-section split Hopkinson pressure bar (SHPB) test system with active confining pressure loading device was used to carry out impact compression and splitting tests on cemented sand specimens. The impact test results show that (1) the prediction value on the fragmentation degree of cemented sand specimens by using the fractal model is basically consistent with the screening results of actual test, which verifies the applicability of the fractal calculation model given in this study; (2) the more the fracture energy dissipated in the crushing process of cemented sand specimens, the more serious the fragmentation degree is, and accordingly the larger the fractal dimension is, that is, the fracture energy is positively correlated with the fractal dimension; (3) there is an exponential relationship between the fractal dimension and energy dissipation of cemented sand specimens under initial stress, which is so different from that under no initial stress. The experimental results in this study can be used to modify the fractal damage model for rock blasting considering the initial stress.

1. Introduction

In order to effectively control and obtain ideal blasting effect, it is necessary to describe the mechanical process of rock blasting mathematically and carry out theoretical research on rock blasting. With the gradual deepening of people's understanding of rock blasting process, three kinds of rock failure criteria, namely, elastic failure, fracture failure, and damage failure, have appeared successively in the study of blasting theory.

Sandia National Laboratory of the United States started the research work of damage model for rock blasting to predict the damage and failure process of rock under explosion load as early as 1966 [1]. The main method is to treat the dynamic fracture of rock as a continuous damage accumulation process, and the basic point is to establish the relationship between damage variable and the density of microcracks in rock.

Due to the fact that the failure process of rock blasting reflected by the damage failure criterion is closer to the reality, it was widely used in the current theoretical research of rock blasting [2–9].

In fact, the discontinuous interfaces such as joints, cracks, holes, and weak surfaces widely existing in the rock are the most critical factors affecting the rock blasting fracture effect [10–12]. Hence, there is inevitable error between the calculation results in rock blasting design and the actual blasting effect in a certain range caused by these factors.

With the further understanding on rock materials, the macroscopic fracture of rock is the final result of the continuous initiation, development, expansion, aggregation, and transfixion of its internal defects. This process from microscopic damage to macroscopic fracture is a process of energy dissipation and has fractal properties. Both the

geometric features of structural evolution and the digital features of mechanical or physical evolution show good statistical self-similarity, such as the fracture mode, crack density, fracture toughness, and fracture surface morphology of the microstructure, etc. The experimental observation showed that the macroscopic fracture of materials was formed by concentration of small fracture groups, and the small fracture was derived from evolution and aggregation of smaller cracks. This behavior of self-similarity inevitably leads to the fragmentation degree after crushing and energy dissipation also having self-similar characteristics [13].

Based on the fractal theory, Yang and Wang [14] incorporated natural rock crack and its evolution law into the rock blasting damage model to develop a new numerical calculation model for rock blasting. The law for crack propagation of rock blasting obtained by numerical calculation with this model is closer to that in engineering practice. Fractal damage model of rock blasting is put forward based on the following viewpoints: the core factors affecting the process and results of rock blasting are macroscopic defects existing in the rock, such as joints and cracks; there is an inseparable relationship between macroscopic defects of rock and its microscopic damage; fractal dimension can be used as a relatively simple holographic stability parameter to describe damage and its evolution, and it is based on the relationship between energy dissipation rate generated by damage and fractal dimension (damage evolution is the process of energy dissipation).

However, the current blasting engineering gradually advances to the deep rock mass in high in-situ stress environment, which inevitably leads to the difference in the blasting fracture theory and surrounding rock stability mechanism compared with that in shallow rock mass [15–19], and the corresponding relationship between energy dissipation rate generated by damage and fractal dimension will also be changed. Therefore, it is of great significance to establish the relationship between fractal dimension and energy dissipation of rock under initial stress, so as to develop a numerical calculation model of rock blasting crack propagation considering initial in-situ stress.

In this study, the impact dynamics tests were carried out on the cemented sand specimens under confining pressure, and the energy dissipation and fractal dimension were calculated and analyzed according to the screening results of fragmentation degree of specimens under impact load, so as to establish the relationship between fractal dimension and energy dissipation.

2. Fractal Calculation Model

The fractal property of rock fragmentation distribution can be understood from two aspects. On the one hand, it has been proved by experiments that the fragmentation process had self-similarity with the shape of rock block and the size distribution of fragment featured power-law, which is a fractal in statistical sense; on the other hand, the analysis of rock microstructure shows that holes and fractures in rock meso-structure are in fractal distribution, and the fragmentation is the direct result of fracture expansion. Therefore, fractal pore rock structure leads to fractal fragmentation distribution, which has inherent and inevitable relation [20–22].

It is assumed that the volume of the fracture model of rock mass is always constant in the process of explosive impact, and the original block is divided into sub-first-order blocks with probability f and similarity ratio r $(0 < x < r)$, at each time when the new blocks are formed. When the original block is divided into sub-first-order blocks after infinite times of repetition, a series of large and small rock blocks with similar shapes are generated [23]. In this process, the reproduction quantity of sub-first-order blocks is $N = (1/r)^3 f$, then the dimension D_f of rock mass group is

$$D_f = \frac{\log N}{\log(1/r)} = 3 - \frac{\log N}{\log r}. \tag{1}$$

If the rock mass is initially composed of M source blocks with line size x_m, the volume of each source block is

$$V = C_V x_m^3, \tag{2}$$

where C_V is the volume shape coefficient.

Then, the line size of the k-order block produced by all the source blocks after k-order fractal construction is

$$x_k = r^k x_m, \quad (k = 0, 1, \ldots), \tag{3}$$

and its number is

$$N_k = \left[\left(\frac{1}{r}\right)^3 f\right]^k (1 - f)M. \tag{4}$$

According to equations (2)–(4), the volume of k-order block is

$$v_k = C_V x_k^3 N_k = C_V x_m^3 f^k (1 - f)M. \tag{5}$$

The total volume of fragmentation with line size less than or equal to x_i is

$$V_i = \lim_{j \longrightarrow \infty} \sum_{k=i}^{j} v_k = C_V x_m^3 f^i M. \tag{6}$$

The volume sum of all blocks is $V_t = \mathrm{MV} = C_V x_m^3 M$, so the ratio of the volume (mass) of blocks with line size less than or equal to x_i to the total volume (mass) is

$$y_i = \frac{V_i}{V_t} = f^i. \tag{7}$$

From equation (3),

$$i = \frac{\log(x_i/x_m)}{\log r}, \tag{8}$$

$$\log f^{((\log(x_i/x_m))/\log r)} = \left(\frac{\log(x_i/x_m)}{\log r}\right)\log f = \left(\frac{\log f}{\log r}\right)\log \cdot \left(\frac{x_i}{x_m}\right) = \log\left(\frac{x_i}{x_m}\right)^{(\log f/\log r)}. \tag{9}$$

It can be deduced from identity transformation equation (9) that

$$f^{((\log(x_i/x_m))/\log r)} = \left(\frac{x_i}{x_m}\right)^{(\log f/\log r)}. \quad (10)$$

Therefore, it can be deduced from equations (1), (7), (8), and (10) that fragmentation distribution obtained from fractal construction is

$$y_i = \left(\frac{x_i}{x_m}\right)^{3-D_f}. \quad (11)$$

The slope of the regression line in a double logarithm coordinate system of $y_i \sim (x_i/x_m)$, which can be established by equation (11), is $b = 3 - D_f$. In this way, the fractal dimension of fragmentation degree (D_f) can be calculated [24].

3. SHPB Test

3.1. Test Apparatus. The SHPB test apparatus system was used in the test, as shown in Figure 1, which is located in the Impact Dynamics Laboratory of Anhui University of Science and Technology. A ∅50 mm variable cross-section steel pressure bar including impact bar, incident bar, and transmission bar was selected from this laboratory for this impact test, all of which were all made of the same type of high-strength alloy steel. The lengths of impact bar, incident bar, and transmission bar are 800 mm, 2,400 mm, and 1,200 mm, respectively, and the elastic modulus, density, and elastic wave velocity are 210 GPa, 7,800 kg/m^3, and 5,190 m/s, respectively. In order to make the front edge of the incident wave rose slowly, a right conic variable cross-section for transition was adopted at the incident end of incident bar, which was quite helpful for constraining the untimely fracture of fragile materials such as rocks and improving the stress uniformity of the specimens [25, 26]. In addition, a device of stress loading was used in conjunction with the SHPB to provide active confining pressure on specimens, as shown in Figure 2.

The cemented sand substitute featured a low wave impedance, which leads to the weaker transmission signals from transmission bar compared with the incident signals from incident bar. Therefore, a semiconductor strain gauge was used to measure weak transmission signals, and a resistance strain gauge was used for the incident bar. In order to improve the loading waveform of the incident pulse and prolong the rising period of the incident pulse, a piece of paper [27] was used as a pulse shaper and pasted on the end of the incident bar.

The stress-strain at both ends of the specimens tended to gradually move towards equilibrium after several transmissions and reflections of stress wave in the specimens according to the basic assumptions [28, 29] of SHPB test technology. On this basis, the dynamic mechanical parameters such as stress $\sigma(t)$, strain $\varepsilon(t)$, and strain rate $\dot{\varepsilon}(t)$ could be calculated according to the following equations:

Figure 1: SHPB test apparatus system.

Figure 2: Device for active confining pressure loading.

$$\sigma(t) = \frac{E_0 A_0}{2A_s}\left[\varepsilon_I(t) + \varepsilon_R(t) + \varepsilon_T(t)\right],$$

$$\varepsilon(t) = -\frac{C_0}{L_s}\int_0^\tau \left[\varepsilon_I(t) + \varepsilon_R(t) - \varepsilon_T(t)\right]\mathrm{d}t, \quad (12)$$

$$\dot{\varepsilon}(t) = -\frac{C_0}{L_s}\left[\varepsilon_I(t) + \varepsilon_R(t) - \varepsilon_T(t)\right],$$

where A_0 and A_s are the cross-section areas of the pressure bar and the specimens, respectively; E_0 and C_0 are the elastic modulus of the pressure bar and the longitudinal wave velocity, respectively; L_s is the length of the specimen; $\varepsilon_I(t)$, $\varepsilon_R(t)$, and $\varepsilon_T(t)$ are the incident, reflected, and transmitted stress waves, respectively. The compressive stress is positive; t is the duration of the stress wave.

The waveforms of incident wave, reflected wave, and transmitted wave are measured during the test, as shown in Figure 3. There was a basically flat section on the reflected wave, which reflects the realization of the constant strain rate loading of the material [24].

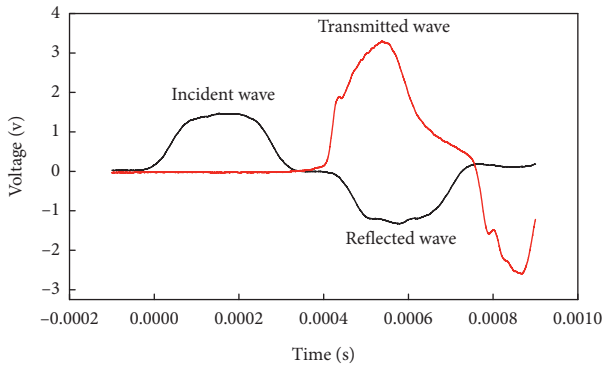

Figure 3: Acquisition waveform of impact compression test.

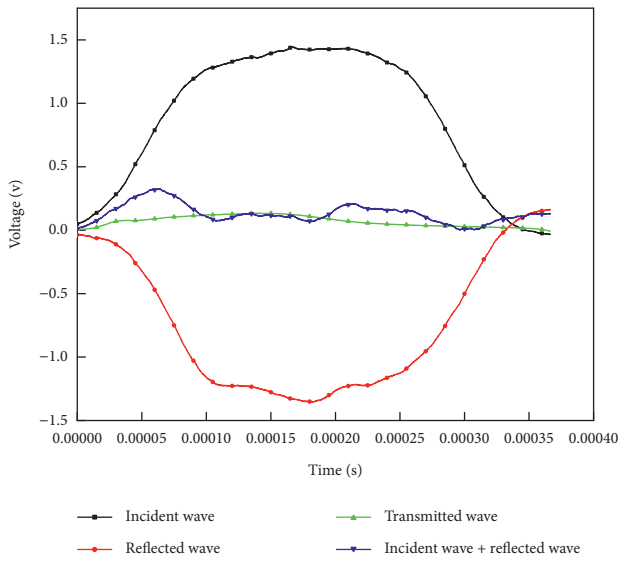

Figure 4: Stress equilibrium diagram.

According to both incident signal and reflection signal, the stress-time curve of the interface between incident bar and specimen can be calculated ("incident + reflection"). According to the transmission signal, the stress-time curve ("transmission") of the interface between the transmission bar and specimen can be calculated. As can be seen from Figure 4, the stress at both ends of the specimen in the test was approximately equilibrium during the whole process of loading [30].

3.2. Rock-Like Material. Impact dynamics tests carried out on real rock specimens under confining pressure showed that when confining pressure is loaded to 20 MPa or more, the specimens were intact and not damaged, which results in impossible calculation of the parameters such as fractal dimension of rock failure and fracture damage energy.

According to the study [31], cemented sand substitute showed good elastic-plastic performance under uniaxial compression, with obvious segmental stress-strain curves, stable post-peak softening section, stable residual strength, and similar failure forms, to real rocks. Therefore, the impact specimens were made of cemented sand substitute. The bulk density of cemented sand substitute is about 18.2 kN/m^3. It is made up of quartz sand as aggregate, gypsum powder as regulator (adding gypsum to the simulated cemented sand can greatly change its mechanical properties, such as reducing its strength and hardness. [32]), and cement as the cementing agent.

In order to extend the model test results to apply in the prototype entity [33], it is necessary to determine the proportional relationship (similarity coefficient) between the prototype and the physical quantities of the model, which is usually expressed by C. To consider the sizes of the engineering prototype and loading apparatus, geometric similarity coefficient C_L was determined to be 20. According to the bulk densities of cemented sand substitute and the prototype rock mass (26 kN/m^3), the similarity coefficient of the bulk density of natural material was obtained that $C_r = 1.42$, and the stress similarity coefficient was $C_\sigma = C_L \times C_r = 28.4$.

Under the conditions that stress similarity coefficient and primary rock strength were 28.4 and 135 MPa, respectively, it was calculated that the strength of the model similar material used in this test should be 4.75 MPa. The strength of the specimen made with proportion of 1:0.095:0.05:0.10 for sand:cement:gypsum:water was able to meet the strength requirement for model similar material. The basic physical parameters of the specimens were measured after 21 days of natural drying conditions at room temperature (20°C) [34], as shown in Table 1.

3.3. Specimens Making. In order to satisfy the stress uniformity requirement of the specimens and mitigate the effect of inertia on the SHPB test, the method [35] recommended by the International Society for Rock Mechanics (ISRM) and the *Method for Determining Physical and Mechanical Properties of Coal and Rock* [36] (China) was used to make the specimens. Therefore, specimens of ∅50 × 25 mm cylinders were prepared to perform dynamic split tests and dynamic compression tests [37–40]. A customized test mold (Figure 5) was used for making the cemented sand specimens, which was considering that the cemented sand specimens were liable to be damaged during mold removal. Some specimens used in the test are shown in Figure 6.

3.4. Test Design. The test comprised both a dynamic tensile test and a dynamic compression test. The dynamic tensile test was designed to calculate the fragmentation energy consumption factor of the specimens, while the dynamic compression test was designed to obtain the relationship between confining pressure and fragmentation fracture energy. Different loading rates were applied by adjusting the impact pressure during the test. Three parallel specimens were selected for each group during the test.

It is known that the buried depth and bulk density of the simulated rock mass were $H = 750$ m and $\gamma = 26$ kN/m^3, respectively, and the horizontal lateral pressure coefficient of the in-situ stress was 1.5. So, based on the vertical stress, $\sigma_v = \gamma H$, σ_v was calculated at 19.5 MPa; based on the average horizontal stress $\sigma_{\text{hav}} = \sigma_v \times 1.5$, σ_{hav} was found to be

Table 1: Physicomechanical parameters of prototype rock and cemented sand substitute.

Material type	γ (kN · m^{-3})	E (GPa)	C (MPa)	φ (°)	μ	σ_c (MPa)	σ_t (MPa)
Primary rock	26	12.97	10.00	43	0.268	135	21.5
CS substitute	18.2	0.36	0.28	43	0.268	4.75	0.603

Note. γ, bulk density; E, deformation modulus; C, cohesion; φ, internal friction angle; μ, poisson's ratio; σ_c, compressive strength; σ_t, tensile strength.

Figure 5: Specimen mold.

Figure 6: Cemented sand specimen.

29.25 MPa; based on the mean stress $\sigma_{av} = ((\sigma_v + \sigma_{hav})/2)$, σ_{av} was determined to be 24.375 MPa, and the simulated confining pressure value was $\sigma = (\sigma_{av}/C_\sigma) = 0.858$ MPa. Therefore, six confining pressure stress values were utilized in this test design, namely, 0.7 MPa, 0.86 MPa, 1.0 MPa, 1.15 MPa, 1.3 MPa, and 1.45 MPa. For other design parameters, see Table 2.

4. Test Results and Discussion

4.1. Results Analysis. The fragments after SHPB dynamic compression test on cemented sand specimens were collected, which were screened into 13 grades with 0~0.15, 0.15~0.3, 0.3~0.6, 0.6~1.18, 1.18~2.36, 2.36~4.75, 4.75~9.5, 9.5~13.2, 13.2~16, 16~26.5, 26.5~31.5, 31.5~37.5, and 37.5~50 mm based on its fragment size. So, according to the

Table 2: SHPB test design.

Test category	Impact air pressure (MPa)	Confining pressure (MPa)	Number of test pieces
Dynamic tension	0.08, 0.1, 0.12, 0.14, 0.16	0	15
Dynamic compression	0.15, 0.2, 0.25, 0.3	0	12
	0.35, 0.50, 0.65, 0.80	0.7/0.86/1.0/ 1.15/1.3/1.45	72

results of fragment screening test of cemented sand after impact compression failure, the fracture energy (W_F) used to form the fracture surface and cause cemented sand crushing and the fractal dimension of fragmentation degree (D_f) was calculated (calculation methods for energy consumption factor and energy dissipation rate were referred to Xu et al.'s study [15]). The calculation results are shown in Table 3.

It can be seen from Table 3 that, under the condition with no confining pressure, both the fracture energy density ($\overline{W}_F$) and fractal dimension of fragmentation degree (D_f) of the cemented sand specimens subjected to impact load increased with the increase of impact pressure, while the damage energy density ($\overline{W}_D$) decreased with increasing impact pressure. Under the same impact pressure, the fracture energy density ($\overline{W}_F$) was larger than the damage energy density ($\overline{W}_D$). This indicated that, under the condition with no confining pressure, there was a positive correlation between fracture energy density ($\overline{W}_F$) and fractal dimension of fragmentation degree (D_f), while there was a negative correlation between damage energy density ($\overline{W}_D$) and fractal dimension of fragmentation degree (D_f), and the energy absorbed by the specimens was mainly used to form the fracture surface.

Under the condition of confining pressure, the fracture energy density ($\overline{W}_F$), fragmentation degree (D_f), and damage energy density ($\overline{W}_D$) of cemented sand specimens subjected to impact load all increased with the increase of impact pressure, and the fracture energy density ($\overline{W}_F$) is less than the damage energy density ($\overline{W}_D$) under the same impact pressure. This indicated that, under confining pressure, the fracture energy density ($\overline{W}_F$) and damage energy density ($\overline{W}_D$) of cemented sand specimens were positively correlated with the fractal dimension of fragmentation degree (D_f), and the energy absorbed by the specimens was mainly used for crack propagation and microcrack damage. The experimental results also demonstrated that under the same impact pressure, the larger the confining stress loaded to the specimen, the smaller the fractal dimension of

Table 3: Fracture damage energy and fracal dimension of fragmentation degree of specimens.

Number	p (MPa)	v (m · s^{-1})	C_p (MPa)	W_F (J)	W_D (J)	$\overline{W}_F$ (10^{3}J · m^{-3})	$\overline{W}_D$ (10^{3}J · m^{-3})	D_f
DY-2-2	0.15	3.11	0	1.752	4.595	35.69	93.61	2.308
DY-2-6	0.2	3.72	0	3.554	3.931	72.40	80.08	2.493
DY-2-9	0.25	4.22	0	5.024	3.154	102.4	64.25	2.714
DY-2-12	0.3	4.80	0	10.39	2.510	211.7	51.13	2.919
WY-1-1-0.7	0.35	6.162	0.7	0.2396	22.76	4.881	463.7	1.208
WY-2-1-0.7	0.5	8.396	0.7	1.399	33.89	28.50	690.4	1.269
WY-3-2-0.7	0.65	9.255	0.7	10.36	49.44	211.0	1007	1.472
WY-4-1-0.7	0.8	10.633	0.7	15.59	51.98	317.6	1059	1.573
WY-1-3-0.86	0.35	6.214	0.86	0.2396	19.76	4.881	402.5	1.194
WY-2-3-0.86	0.5	7.862	0.86	1.281	28.60	26.10	582.6	1.201
WY-3-1-0.86	0.65	9.314	0.86	7.960	44.51	162.2	906.8	1.397
WY-4-1-0.86	0.8	10.789	0.86	14.44	51.83	294.2	1056	1.411
WY-1-3-1	0.35	6.282	1	0.2396	15.32	4.881	312.1	1.072
WY-2-3-1	0.5	8.205	1	1.152	26.46	23.47	539.0	1.132
WY-3-2-1	0.65	9.325	1	7.011	43.88	142.8	893.9	1.265
WY-4-3-1	0.8	10.679	1	14.10	46.25	287.2	942.2	1.352
WY-1-1-1.15	0.35	6.47	1.15	0.2396	13.63	4.881	277.7	0.9844
WY-2-1-1.15	0.5	8.154	1.15	1.107	21.17	22.55	431.3	1.012
WY-3-1-1.15	0.65	9.325	1.15	6.037	39.39	123.0	802.4	1.195
WY-4-2-1.15	0.8	10.764	1.15	10.28	48.45	209.4	987.0	1.216
WY-1-3-1.3	0.35	6.282	1.3	0.2396	12.34	4.881	251.4	0.8812
WY-2-1-1.3	0.5	7.681	1.3	0.8404	16.01	17.12	326.4	0.9091
WY-3-1-1.3	0.65	9.422	1.3	4.954	30.34	100.9	618.1	0.9852
WY-4-3-1.3	0.8	10.638	1.3	6.986	42.64	142.3	868.7	1.138
WY-1-1-1.45	0.35	6.447	1.45	0.2396	9.440	4.881	192.3	0.6531
WY-2-2-1.45	0.5	8.202	1.45	0.6897	14.50	14.05	295.4	0.6731
WY-3-3-1.45	0.65	9.847	1.45	2.436	32.02	49.63	652.3	0.7992
WY-4-3-1.45	0.8	11.546	1.45	4.955	38.99	100.9	794.3	1.119

Note. Number, specimen number; p, impact air pressure; v, impact velocity; C_p, confining pressure values; W_F, fracture energy; W_D, damage energy; $\overline{W}_F$, fracture energy density; $\overline{W}_D$, damage energy density; D_f, fractal dimension of fragmentation degree. The fracture energy density and damage energy density shown in the table are respectively the fracture energy and damage energy dissipated by cemented sand specimens per unit volume, which are defined to study the relationship between fractal dimension of fragmentation degree and fracture energy, damage energy dissipated by specimens.

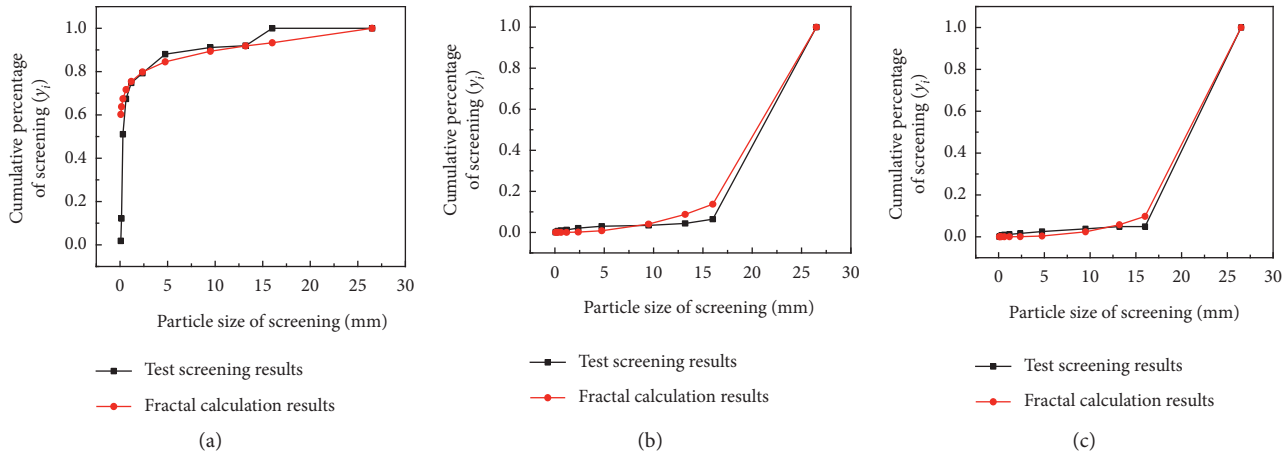

Figure 7: Predicted value and test screening results of fragmentation degree.

fragmentation degree (D_f), that is, the less serious the fragmentation.

In order to verify the correctness of "fractal calculation model" derived in the second section of this study, three specimens' screening results of fragments selected from tests and its fractal dimension values calculated by the model are shown in Figure 7 for comparative analysis.

Figures 7(a)–7(c) showed the comparison between predicted values for rock fragmentation by using the block-fractal model and experimental screening results under the confining pressures with 0 MPa, 1.3 MPa, and 1.45 MPa, respectively. By comparison, it was found that the calculation results by fractal model in Figures 7(a)–7(c) were basically consistent with the experimental screening results,

which proved that the fractal evolution characteristics of rock fracture and the fractal model of rock fracture fragmentation derived in the second section of this study were correct.

4.2. Relationship between Fractal Dimension of Fragmentation Degree and Energy Dissipation. The data in Table 3 of fracture energy density ($\overline{W}_F$) and fractal dimension of fragmentation degree (D_f) are shown in Figures 8 and 9.

Goodness of fit refers to the fitting degree of regression line to the observed value. The statistic that measures goodness of fit is the determination coefficient (R^2). The closer the value of R^2 to 1, the better the fitting degree of regression line to the observed value; conversely, the smaller the value of R^2, the worse the fitting degree of regression line to the observed value.

The data points of fracture energy density and fractal dimension of fragmentation degree under and without confining pressure were fitted with the smooth curves of linear, polynomial, logarithmic, power, and exponential functions, and the curves of relation between fracture energy density and fractal dimension of fragmentation degree of different types are drawn, respectively. By comparing determination coefficients, it can be obtained that the relationship between fracture energy density and fractal dimension of fragmentation degree is approximately linear function under the condition of no confining pressure, and the relationship between fracture energy density and fractal dimension of fragmentation degree is approximately exponential function under the condition of confining pressure. The fitting curves are shown in Figures 8 and 9 and the relationship between fracture energy density ($\overline{W}_F$) and fractal dimension of fragmentation degree (D_f) can be obtained as follows:

Confining pressure with 0 MPa,

$$D_f = 2.26 + 0.00332\overline{W}_F, \quad R^2 = 0.9056. \tag{13}$$

Confining pressure with 0.7 MPa,

$$D_f = 1.90 - 0.689e^{-0.00232\overline{W}_F}, \quad R^2 = 0.996. \tag{14}$$

Confining pressure with 0.86 MPa,

$$D_f = 1.436 - 0.271e^{-0.00970\overline{W}_F}, \quad R^2 = 0.971. \tag{15}$$

Confining pressure with 1.0 MPa,

$$D_f = 1.40 - 0.329e^{-0.00651\overline{W}_F}, \quad R^2 = 0.993. \tag{16}$$

Confining pressure with 1.15 MPa,

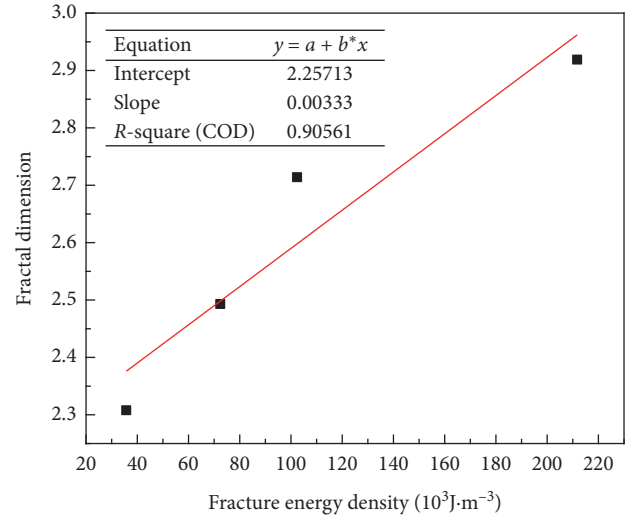

Figure 8: The relationship between fractal dimension and fracture energy density without confining pressure.

$$D_f = 1.24 - 0.287e^{-0.0126\overline{W}_F}, \quad R^2 = 0.987. \tag{17}$$

Confining pressure with 1.3 MPa,

$$D_f = 0.878 + 0.01298e^{0.02105\overline{W}_F}, \quad R^2 = 0.993. \tag{18}$$

Confining pressure with 1.45 MPa,

$$D_f = 0.470 + 0.1699e^{0.01328\overline{W}_F}, \quad R^2 = 0.999. \tag{19}$$

According to the above equations, the variation law of $\overline{W}_F$ andD_f in the figures can be further summarized as follows:

When $C_p = 0$ MPa, the linear relationship between $\overline{W}_F$ andD_f was as follows:

$$D_f = A_1 + A_2\overline{W}_F. \tag{20}$$

When $C_p \neq 0$ MPa, the exponential relationship between $\overline{W}_F$ andD_f was as follows:

$$D_f = A_1 - A_2e^{-k\overline{W}_F}, \tag{21}$$

where A_1 represented the ultimate fractal dimension;A_2 and k were parameters related to the confining pressure.

This indicated that the relationship between fractal dimension of fragmentation degree (D_f) and fracture energy density ($\overline{W}_F$) also changed from linear to exponential function with the change from zero to nonzero of confining pressure constraint state.

The fractal damage model for rock blasting deduced in reference [41] was exactly established on the linear proportional relationship between fractal dimension and

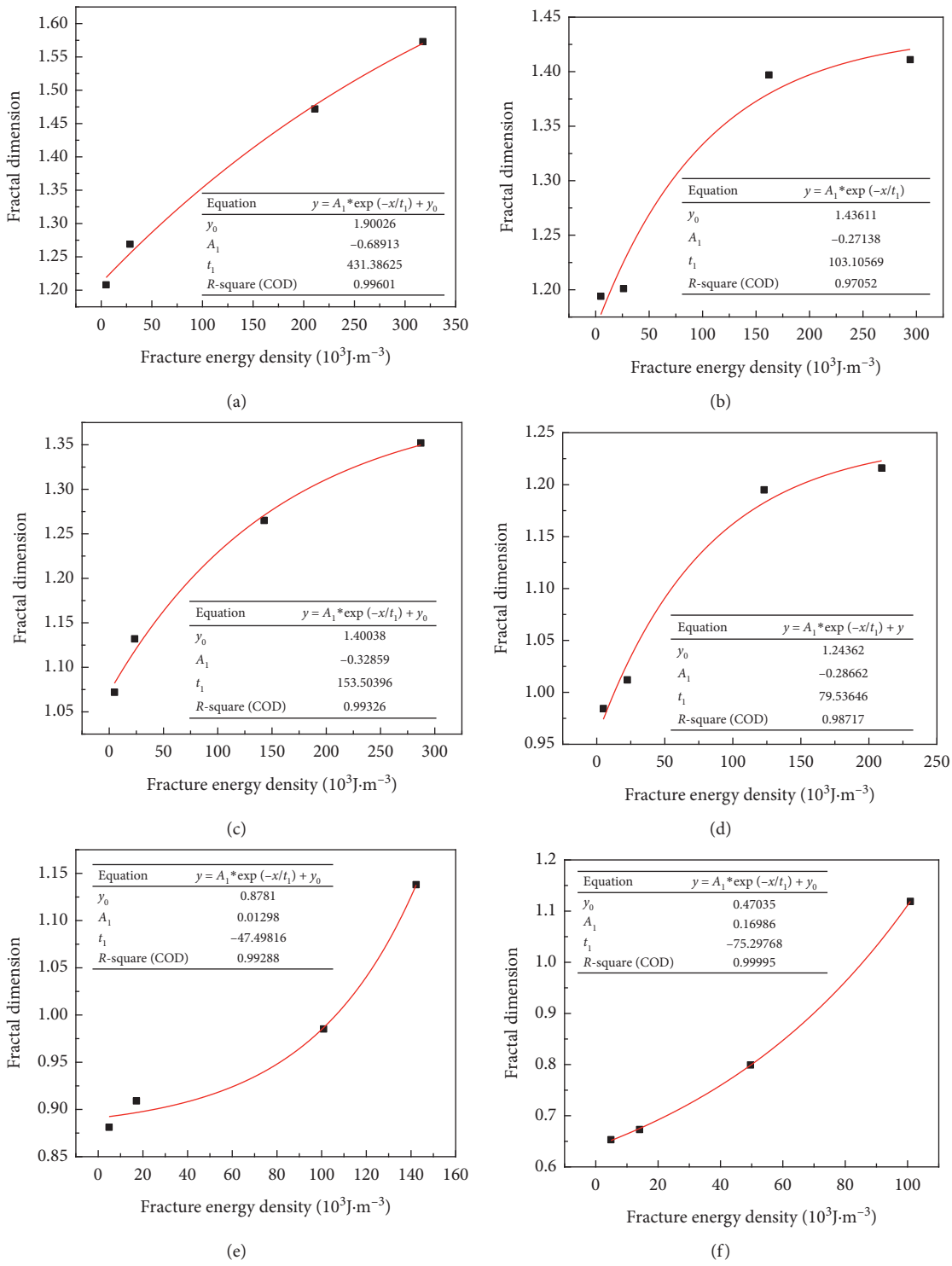

Figure 9: The relationship between fractal dimension and fracture energy density under confining pressure, (a) 0.7 MPa, (b) 0.86 MPa, (c) 1.0 MPa, (d) 1.15 MPa, (e) 1.3 MPa, and (f) 1.45 MPa.

fracture (or damage) dissipation energy of the rock failure process under no initial stress (i.e., equation (20)).

The results of this study showed that the energy dissipation rate was greatly affected by in-situ stress. Therefore, the fractal damage model for rock blasting considering initial stress needed to be established on the relationship between fractal dimension and fracture (or damage) dissipation energy of the rock failure process under initial stress state, i.e., equation (21), which can be expressed as

$$D_f = D_0 + K_1 e^{-K_2 Y}, \tag{22}$$

where D_0 represented the fractal dimension of initial rock crack; K_1 and K_2 were parameters determined by experiment (related to initial stress); D_f represented fractal dimension of rock fragmentation degree in blasting process; Y represented the energy dissipation rate of rock fracture or damage.

By substituting equation (22) into the fractal damage model for rock blasting deduced in reference [41], the fractal damage model for rock blasting considering initial stress can be obtained.

5. Conclusions

According to this study, under the condition that without confining pressure, the energy absorbed by the cemented sand specimens was mainly used to form the fracture surface. Under the condition that with confining pressure, the energy absorbed by cemented sand specimens was mainly used for crack propagation and microcrack damage. The more the fracture energy dissipated, the more serious the fracture degree and the larger the corresponding fractal dimension will be. Under the same impact pressure condition, the greater the confining stress loaded to the specimens, the smaller the fractal dimension of fragmentation degree (D_f), that is, the less serious the fracture degree.

In addition, it was also concluded from this study that there was a positive correlation between fractal dimension (D_f) and fracture energy density $\overline{W}_F$. However, the energy dissipation rate was greatly affected by in-situ stress, so the relationships between D_f and $\overline{W}_F$ were quite different with each other under different confining pressures. Without confining pressure, the relationship between them is linear, while under confining pressure, the relationship between them is exponential. Therefore, according to the relationship between fractal dimension (D_f) and fracture energy density ($\overline{W}_F$) under confining pressure, a fractal damage model for rock blasting considering initial stress can be established.

Despite some important conclusions drawn from this study, due to the fact that the rock-like specimens used in the test were made of homogeneous materials, which were different from the rocks with the characteristics of anisotropism in practical engineering, there were inevitable errors in the research results. Therefore, the technology of 3D printing can be used in further research to develop rock-like materials more in line with the real rock for the study of rock impact dynamics.

Nomenclature

f: Probability
r: Similarity ratio
N: Reproduction quantity of sub-first-order blocks, $N = (1/r)^3 f$
D_f: Dimension of rock mass group
M: Number of source blocks
Line size
x_m,
x_i:
V: Volume of each source block
b: Slope of the regression line
C_V: Volume shape coefficient
k: Number of fractal construction
V_i: Total volume of fragmentation with line size less than or equal to x_i
N_k: Number of k-order block
v_k: Volume of k-order block
V_t: Volume sum of all blocks
y_i: Ratio of the volume (mass) of blocks.

Data Availability

The datasets generated and analyzed during the current study are available from the corresponding author upon reasonable request.

Conflicts of Interest

The authors declare that there are no conflicts of interest regarding the publication of this paper.

Acknowledgments

The authors extend their gratitude to the National Natural Science Foundation, China (51374012) and Anhui Province Science and Technology Project, China (1501041123). Those supports are gratefully acknowledged.

References

[1] X. Yang and S. Wang, "Rock blast damage models and comments," *Engineering Blasting*, vol. 5, no. 3, pp. 71–75, 1999, in Chinese.

[2] D. E. Grady and M. E. Kipp, "Continuum modelling of explosive fracture in oil shale," *International Journal of Rock Mechanics and Mining Sciences & Geomechanics Abstracts*, vol. 17, no. 3, pp. 147–157, 1980.

[3] L. M. Taylor, E.-P. Chen, and J. S. Kuszmaul, "Microcrack-induced damage accumulation in brittle rock under dynamic loading," *Computer Methods in Applied Mechanics and Engineering*, vol. 55, no. 3, pp. 301–320, 1986.

[4] B. Budiansky and R. J. O'connell, "Elastic moduli of a cracked solid," *International Journal of Solids and Structures*, vol. 12, no. 2, pp. 81–97, 1976.

[5] J. S. Kuszmaul, "A new constitution model for fragmentation of rock under dynamic loading," in *Proceedings of the 2nd International Symposium on Rock Fragmentation by Blasting*, pp. 412–423, Keystone, CO, USA, August 1987.

[6] B. J. Thorne, P. J. Hommert, and B. Brown, "Experimental and computational investigation of the fundamental mechanisms of cratering," in *Proceedings of the 3rd International Symposium on Rock Fragmentation by Blasting*, pp. 117–122, Brisbane, Australia, August 1990.

[7] R. Yang, W. F. bawden, and P. D. Katsabanis, "A new constitutive model for blast damage," *International Journal of Rock Mechanics and Mining Sciences & Geomechanics Abstracts*, vol. 33, no. 3, pp. 245–254, 1996.

[8] L. Liu and P. D. Katsabanis, "Development of a continuum damage model for blasting analysis," *International Journal of Rock Mechanics and Mining Sciences*, vol. 34, no. 2, pp. 217–231, 1997.

[9] C. Tang, "Numerical simulation of progressive rock failure and associated seismicity," *International Journal of Rock Mechanics and Mining Sciences*, vol. 34, no. 2, pp. 249–261, 1997.

[10] P. Qiu, Z. Yue, Y. Ju, and J. Zhao, "Characterizing dynamic crack-tip stress distribution and evolution under blast gases and reflected stress waves by caustics method," *Theoretical and Applied Fracture Mechanics*, vol. 108, Article ID 102632, 2020.

[11] P. Qiu, Z. Yue, R. Yang, and J. C. Li, "Effects of vertical and horizontal reflected blast stress waves on running cracks by caustics method," *Engineering Fracture Mechanics*, vol. 212, pp. 164–179, 2019.

[12] Z. Yue, P. Qiu, R. Yang, S. Zhang, K. Yuan, and Z. Li, "Stress analysis of the interaction of a running crack and blasting waves by caustics method," *Engineering Fracture Mechanics*, vol. 184, pp. 339–351, 2017.

[13] Y. Tan, C. Liu, and T. Zhao, *Initial Theory of Rock Nonlinear Dynamics*, Coal Industry Press, Beijing, China, 2008.

[14] J. Yang and S. Wang, "Research on fractal damage model for rock blasting," *Explosion and Shock Waves*, vol. 16, no. 1, pp. 5–10, 1996, in Chinese.

[15] Y. Xu, J. Ge, and W. Huang, "Energy analysis on dynamic fragmentation degree of cemented sand specimens under confining pressure," *Shock and Vibration*, vol. 2019, Article ID 5893957, 12 pages, 2019.

[16] C. Yi, D. Johansson, and J. Greberg, "Effects of in-situ stresses on the fracturing of rock by blasting," *Computers and Geotechnics*, vol. 104, pp. 321–330, 2017.

[17] A. Mazaira and P. Konicek, "Intense rockburst impacts in deep underground constructions and their prevention," *Canadian Geotechnical Journal*, vol. 52, no. 10, 2015.

[18] L. B. Jayasinghe, J. Shang, Z. Zhao et al., "Numerical investigation into the blasting-induced damage characteristics of rocks considering the role of in-situ stresses and discontinuity persistence," *Computers and Geotechnics*, vol. 116, pp. 1032071–10320712, 2019.

[19] A. Sainoki, M. Z. Emad, and H. S. Mitri, "Study on the efficiency of destress blasting in deep mine drift development," *Canadian Geotechnical Journal*, vol. 54, no. 4, 2017.

[20] H. Xie and F. Gao, "The fractal features of the damage evolution of rock materials," *Chinese Journal of Rock Mechanics and Engineering*, vol. 10, no. 1, pp. 74–82, 1991.

[21] F. Gao, H. Xie, and J. Wu, "Fractal analysis of the relation between rock damage and rock fragmentation," *Chinese Journal of Rock Mechanics and Engineering*, vol. 18, no. 5, pp. 503–506, 1999.

[22] X. Sun, Z. Wu, and Y. Huang, *Fractal Principle and Its Application*, China University of science and Technology Press, Hefei, China, 2006.

[23] Y. Qian, *Experimental Study on Blasting Lumpiness of Jointed Rock Mass Based on Fractal Theory*, Wuhan University of Technology, Wuhan, China, 2005, in Chinese.

[24] J. Xu, J. Fan, and X. Lv, *Dynamic Mechanical Properties of Rock with the Confining Pressure*, Northwestern Polytechnical University press, Xi'an, China, 2012, in Chinese.

[25] X. Liu and S. Hu, "Wave propagation characteristics in cone bars used for variable cross section SHPB," *Explosion and Shock Waves*, vol. 20, no. 2, pp. 110–114, 2000, in Chinese.

[26] Q. Ping, Q. Ma, and P. Yuan, "Prediction for stress equilibrium time in rock SHPB test," *Journal of Vibration and Shock*, vol. 32, no. 12, pp. 55–60, 2013, in Chinese.

[27] X. Wu and D. A. Gorham, "Stress equilibrium in the split Hopkinson pressure bar test," *Journal de Physique IV France*, vol. 7, no. C3, pp. 91–96, 1997.

[28] L. Wang, *Foundation of Stress Waves*pp. 39–64, National Defense Industry Press, Beijing, China, 2010, in Chinese, 2nd edition.

[29] L. Song and S. Hu, "Two wave and three wave method in SHPB data processing," *Explosion and Shock Waves*, vol. 25, no. 4, pp. 368–373, 2005, in Chinese.

[30] F. Y. Lu, R. Chen, Y. L. Lin et al., *Hopkinson Rod Experimental Technology*, Science Press, Beijing, China, 2013.

[31] F. Luo, B.-S. Yang, B.-B. Hao, L.-H. Sun, and M.-M. Fu, "Mechanical properties of similar material under uniaxial compression and the strength error sources," *Journal of Mining and Safety Engineering*, vol. 30, no. 1, pp. 93–99, 2013.

[32] X. Shi, B. Liu, and J. Xiao, "A method for determining the ratio of similar materials with cement and plaster as bonding agents," *Rock and Soil Mechanics*, vol. 36, no. 5, pp. 1357–1362, 2015.

[33] J. Yang, *Similarity Theory and Structural Model Test*, Wuhan University of Technology press, Wuhan, China, 2005, in Chinese.

[34] P. Yuan and Y. Xu, "Influence of curing time on compressive properties of cemented sand similar materials," *Journal of Vibration and Shock*, vol. 34, no. 13, pp. 200–204, 2015.

[35] International Society for Rock Mechanics, "Suggested methods for determining tensile strength of rock materials," *International Journal of Rock Mechanics and Mining Sciences and Geomechanics Abstracts*, vol. 15, no. 1, pp. 99–103, 1978.

[36] The National Standards Compilation Group of People's Republic of China. GB/T 23561-2010, *Methods for Determining the Physical and Mechanical Properties of Coal and Rock*, Standards Press of China, Beijing, China, 2010, in Chinese.

[37] M. Pankow, C. Attard, A. M. Tian et al., "Specimen size and shape effect in split Hopkinson pressure bar testing," *Acta Mechanica Solida Sinca*, vol. 26, no. 1, pp. 107–110, 2005, in Chinese.

[38] F. Gao, J. Yang, Y. Liu et al., "Research on rock parastatic and dynamic impact test and size effect," *Coal Science and Technology*, vol. 37, no. 4, pp. 19–22, 2009, in Chinese.

[39] F. Gong, X. Li, Q. Rao et al., "Reference method for determining sample size in SHPB tests of rock materials," *Journal of Vibration and Shock*, vol. 32, no. 17, pp. 24–28, 2013, in Chinese.

[40] M. Pankow, C. Attard, and A. M. Waas, "Specimen size and shape effect in split Hopkinson pressure bar testing," *The Journal of Strain Analysis for Engineering Design*, vol. 44, no. 8, pp. 689–698, 2009.

[41] J. Yang, Q. Jin, and F. Huang, *Theoretical Model and Numerical Calculation for Rock Blasting*, Science Press, Beijing, China, 1999, in Chinese.